AUT Journal of Mechanical Engineering

AUT J. Mech. Eng., 2(1) (2018) 13-26
DOI: 10.22060/mej.2017.13013.5500

Simulation of Natural Convection in Eccentric Annulus: A Combined Lattice Boltzmann and Smoothed Profile Approach

S. Jafari[1], S. Jafari[2*], M. Rahnama[1]

[1] Mechanical Engineering Department, ShahidBahonar university of Kerman, Kerman, Iran
[2] Petroleum Engineering Department, ShahidBahonar university of Kerman, Kerman, Iran

ABSTRACT: In the present study, a hybrid method of thermal lattice Boltzmann and smoothed profile methods have been applied to simulate free convection in an eccentric annulus with a constant temperature wall. Smoothed profile method employs an Eulerian approach to consider the fluid-solid interaction without using an extra mesh for capturing solid boundary. As a result of this property, the combination of this method and Lattive Boltzmann method can be considered as an efficient method to simulate free convection in complex geometries like annulus. In order to investigate the effect of inner cylinder position on the natural convection, the inner cylinder was placed in different horizontal, vertical and diagonal positions. Influences of the Rayleigh number ($10^3 \leq Ra \leq 10^5$), eccentricity ($-0.75 \leq e \leq 0.75$)) and the radial ratio (R_o/R_i=2, 2.6 and 3.2) on the streamlines, isotherms and Nusselt number were studied. It was found that the Nusselt number has a positive relationship with Rayleigh number and radial ratio. Also, it can be confirmed that Nusselt number in the case with the negative eccentricity (e=−0.75) was larger than the others. It was found that a very good agreement exists between the present results and those from the open literature.

Review History:
Received: 16 June 2017
Revised: 19 October 2017
Accepted: 28 November 2017
Available Online: 10 January 2018

Keywords:
Lattice boltzmann method
Natural convection
Smoothed profile method
Annulus

1- Introduction

Forced and natural convections in annulus occur in many engineering applications, including nuclear reactor design, cooling of electronic equipment and underground electric transmission cables using pressurized gas, thermal storage systems, aircraft fuselage, solar energy systems [1-6]. It has been investigated by various authors both experimentally [1-4] and numerically [4-6], mainly with the aim of enhancing heat transfer between the two cylinders. In a pioneering work, an experimental and theoretical study of natural convection between the two concentric and eccentric horizontal cylinders was performed by Kuhen and Goldsein [2-4]. They investigated the effect of Rayleigh number and eccentricity on natural convection heat transfer in the annulus. Their results are still used by other researchers for validation purposes. Guj and Stella [5] performed numerical and experimental analysis of buoyancy-driven flow in a horizontal annulus. Their numerical simulation was done using finite volume method. The effect of horizontal eccentricity was studied in their work and they found that the average Nusselt number is nearly independent of the horizontal eccentricity. Shahraki et al [6] employed penalty finite element method to simulate natural convection in an annulus between two vertically eccentric pipes with various eccentrics. Moreover, they found out when the hot cylinder is placed high in the outer cold cylinder (high positive eccentricity), the circulation is slower over the annulus and the average Nusselt number decreases. As a consequence, the circulation is faster when the hot cylinder is positioned low in the cold outer cylinder, the average Nusselt number increases. Lattice Boltzmann method (LBM) has attracted great attention in the last decades as a novel approach compared to conventional computational fluid dynamic [7-9]. Various problems were studied using LBM, including natural convection in simple geometries [10-12]. Some authors studied more complex geometries such as natural convection in a cold square enclosure with a heated inner circular cylinder [13-16]. LBM has been also extended to simulate natural convection of nanofluids in an annulus [17]. Moreover, some researchers considered a natural convection of nanofluids with magnetic effects [18].

The geometry of concentric annulus with a heated inner circular cylinder in a cold circular enclosure was also studied in some of them [13,14]. One of the main concerns in these geometries is the application of no-slip and no-temperature jump at the solid-fluid interface, which requires the local fluid velocity and temperature at the boundary to be the same as that of the solid boundary. There are various methods available to treat the no-slip boundary conditions. The simplest way to do this is the standard bounce-back method. The main drawback of this boundary condition is the step-wise representation of the curved boundary [9]. To overcome this drawback, curved boundary condition [19] can be used to implement no-slip boundary condition which needs to interpolate between some lattice nodes inside and outside of the curved boundary. Fattahi et al. [20] presented a numerical simulation of the natural convection heat transfer in eccentric annulus based on the double population LBM using the curved boundary condition. The effect of vertical, horizontal and diagonal eccentricity was investigated in their study.

As the main concern in natural convection, no-slip velocity and temperature boundary conditions and their related heat flux are required to be implemented to get the correct results. Various methods have been proposed to satisfy such boundary conditions, among them, Immersed Boundary Method

Corresponding author, E-mail: jafari@uk.ac.ir

(IBM) has been used successfully in many convection heat transfer geometries. IBM was first introduced by Peskin [21] to model the blood flow in the heart. In the IBM, the fluid equations are discretized on a fixed Eulerian grid over the entire domain while the immersed boundary is discretized on a moving Lagrangian mesh. As both IBM and LBM are based on a Cartesian grid, a combination can be readily applied to simulations of curved boundary problems. The evaluation of the force density at each Lagrangian point can be performed by the penalty method [21], the momentum exchange method [22], or the direct forcing method [23]. Application of IB-LBM to thermal phenomena was extended by incorporating the IBM into the thermal LBM (TLBM) based on the double population approach [15]. In these methods, a source term is added to the energy equation as a source term similar to the force term in the isothermal method. Similar to isothermal problems, the difference between given temperature and computed one was the main idea for calculating heating source term. Seta [15] demonstrated that the immersed-boundary thermal lattice Boltzmann method requires the implicit temperature-correction method in order to use the source term to enhance the accuracy of the temperature equation in the lattice Boltzmann scheme.

Recently, a combination of the LBM and smoothed profile method (SPM) has been introduced as an alternative to simulate particle suspensions [25]. Nakayama and Yamamoto [26] used SPM to simulate particulate flow in their Navier-Stokes solver. Jafari et al. [25] combined SPM and LBM to use the common features of them in order to introduce an efficient approach for simulation of particle suspensions. SPM is based on the definition of a smoothly spreading interface layer which is used to represent the particle boundaries such that a smoothly varying interface is substituted for a sharp one. The proposed method uses fixed Eulerian grids for the host fluid. The curved boundaries are represented by certain smooth-body forces in the discretized Boltzmann equation. SPM-LBM combination solves a single set of fluid dynamics equations for the entire domain, including solid volumes with curved boundaries without any internal boundary conditions or using interpolation to evaluate the body force at fluid nodes. More recently, Hu et al. [27] extended the isothermal LBM-SPM to thermal flow to simulate the forced and natural convection in complex geometries.

In this paper, we aim to study natural convection in an eccentric annulus with constant wall temperature. It should be indicated that the fluid flow and heat transfer phenomena in irregular domain occur frequently in many engineering applications. The boundary treatment for complex boundaries is an important issue in computational fluid dynamics. Compared with the conventional body-fitted, unstructured grid methods and the immersed boundary method (IBM), SPM is a very high efficient method. In the present study, the thermal Smoothed Profile-Lattice Boltzmann Method, SP-TLBM is used to investigate the natural convection in an annulus. Based on literature reviews, no work has focused on investigating the influences of the physical parameters, geometry parameters on flow and heat transfer characteristics in an eccentric cylindrical annulus for different horizontal, vertical and diagonal positions of the inner cylinder.

2- Governing Equations

LBM is a computational procedure based on the solution of Boltzmann equation, from which, macroscopic properties such as density and velocity are obtained. It is a mesoscopic approach with the capability of considering multi-phase situation; but with the assumption of constant temperature. In problems containing heat transfer, there is a temperature variation which is required to be treated separately to satisfy conservation of energy. The method used for the case of heat transfer is called Thermal LBM, TLBM. A detailed discussion about LBM and TLBM is presented in the following sections.

2- 1- Lattice Boltzmann method

LBM is a numerical procedure to solve Boltzmann equation. As the main concept in LBM, density distribution function, $f(x,v,t)$ is obtained from a discretized form of Boltzmann equation which can be expressed as follows:

$$f_i\left(x+\vec{e}_i\delta t, t+\delta t\right)-f_i\left(x,t\right)= -\frac{1}{\tau_f}\left(f_i\left(x,t\right)-f_i^{eq}\left(x,t\right)\right)+\vec{F}_i\delta t \quad (1)$$

Here $f_i(x,t)$ and $f_i^{eq}(x,t)$ are density and equilibrium distribution functions, respectively in $\vec{e}_i$ direction at the position x and time t, δt is time step and τ_f is the relaxation time of momentum equation. $\vec{F}_i$ represents external forces such as fluid-solid interaction force and buoyancy force. Based on D2Q9 model for 2-D lattice Boltzmann method, the discrete velocities $\vec{e}_i$ are defined as: e_0=(0,0); e_i=(±1,0)c and e_i=(0,±1)c for i=1-4 and e_i=(±1,±1)c for i=5-8. Equilibrium distribution function, f_i^{eq}, is given in the following equations:

$$f_i^{eq}=\rho w_i\left(1+3\frac{\vec{e}_i\vec{u}}{c^2}+9\frac{\left(\vec{e}_i\vec{u}\right)^2}{2c^4}-\frac{3\vec{u}\vec{u}}{2c^2}\right) \quad (2)$$

It should be mentioned that c is the streaming speed which is equal to $\delta x/\delta t$ where δx is the lattice spacing and δt is the time step and $c=\sqrt{3}c_s$ where c_s the lattice sound speed. w_i is the weighting coefficient expressed as:

$$w_i=\begin{cases}\frac{4}{9} & i=0\\ \frac{1}{9} & i=1-4\\ \frac{1}{36} & i=5-8\end{cases}$$

τ_f is given as $3\upsilon+0.5$ where υ is the kinematic viscosity.

As mentioned before, F_i represents all external forces. In LBM, it is expressed as:

$$F_i=\omega_i\left(\frac{2\tau_f-1}{2\tau_f}\right)\left(\frac{\vec{e}_i-\vec{u}}{c_s^2}+\frac{\vec{e}_i\vec{u}}{c_s^2}\vec{e}_i\right).\left(\vec{F_H}+\vec{F_E}\right) \quad (3)$$

Where $\vec{F}_E$ stands for any external force except fluid-solid interaction force and $\vec{F}_H$ is the force arises due to the hydrodynamic interactions between fluid and solid regions.

The macroscopic properties of fluid mass density and fluid

velocity can be computed as

$$\rho = \sum_{i=0}^{8} f_i \tag{4}$$

$$\rho \vec{u} = \sum_{i=1}^{8} \vec{e}_i f_i + \frac{1}{2}\left(\vec{F_H} + \vec{F_E}\right)\delta t \tag{5}$$

2- 2- Thermal Lattice Boltzmann method

Heat transfer in the fluid flow is governed by energy conservation equation. A temperature distribution function is defined in LBM for which a similar equation can be expressed as:

$$g_i\left(x + \vec{e}_i \delta t, t + \delta t\right) - g_i\left(x,t\right) = -\frac{1}{\tau_g}\left(g_i\left(x,t\right) - g_i^{eq}\left(x,t\right)\right) + G_i \delta t \tag{6}$$

Here $g_i(x,t)$ and g_i^{eq} are temperature and energy equilibrium distribution functions, respectively. G_i is the heat source or sink term and τ_g is the relaxation time for the thermal field which is defined by $\tau_g = 3\alpha + 0.5$ where α is the thermal diffusivity.

The equilibrium distribution function for temperature field can be defined as:

$$g_i^{eq} = T w_i \left(1 + 3\frac{\vec{e}_i \vec{u}}{c^2} + 9\frac{\left(\vec{e}_i \vec{u}\right)^2}{2c^4} - \frac{3\vec{u}\vec{u}}{2c^2}\right) \tag{7}$$

G_i can be expressed as

$$G_i = \omega_i \left(\frac{2\tau_g - 1}{2\tau_g}\right) Q \tag{8}$$

Where Q is the heat source/sink which is located in solid regions. Eventually, the temperature can be computed using the following equation:

$$T = \sum_{i=0}^{8} g_i + \frac{1}{2} Q \delta t \tag{9}$$

2- 3- Smoothed profile method

Smoothed Profile Method, SPM, is a method of implementing fluid-solid interaction force in any flow geometry containing solid boundaries such as particulate flows. Using SPM, no-slip boundary condition is satisfied while the correct fluid-solid interaction force is recovered. It is based on replacing sharp fluid-solid interface with a function (φ) which is changed continuously through the finite thickness (ε) as depicted in Figure 1. While this function can be written in different forms, the following equation is used in the present computations [25- 27]:

$$\varphi_i\left(x\right) = \begin{cases} 0 & x < \dfrac{-\varepsilon}{2} \\ 0.5\sin\left(\dfrac{\pi x}{\varepsilon} + 1\right) & \dfrac{-\varepsilon}{2} < x < \dfrac{\varepsilon}{2} \\ 1 & x > \dfrac{\varepsilon}{2} \end{cases} \tag{10}$$

As observed from the above relation, this is a function which varies from 0 to 1 with 1 that corresponds to solid particle region and 0 corresponds to the fluid region. If there is more than one particle, a function is defined for each particle, resulting in a density field expressed as:

$$\varphi\left(x,t\right) = \sum_{i=1}^{n} \varphi_i\left(x,t\right) \tag{11}$$

Where n is the number of solid particles.

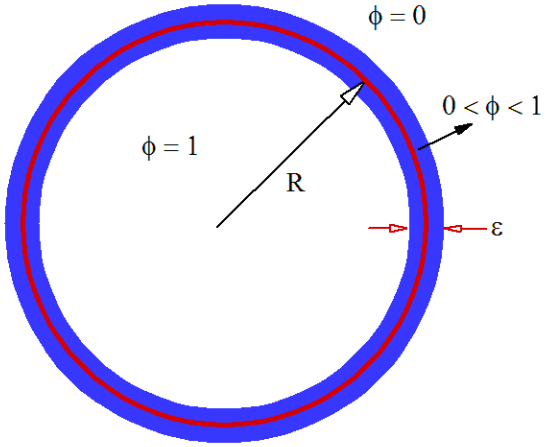

Fig. 1. Fluid-solid interface function

Considering that $\varphi_i = 0$ and $\varphi_i = 1$ represent fluid and solid regions respectively, a velocity field can be defined for the whole computational domain as:

$$\vec{u}\left(x,t\right) = \left(1 - \varphi\right)\vec{u_f}\left(x,t\right) + \varphi\vec{u_p}\left(x,t\right) \tag{12}$$

In the above equation, $u_f(x,t)$ and $u_p(x,t)$ are the velocities in fluid and particle (solid) regions, respectively. A two-steps procedure is used to implement fluid-solid interaction force and obtain subsequent velocity. It consists of (a) neglecting the fluid-solid interaction force and obtaining an intermediate velocity field, u', as:

$$\rho\left(x,t\right)\vec{u'}\left(x,t\right) = \sum_{i=1}^{8} \vec{e}_i f_i\left(x,t\right) + \frac{1}{2}\left(\vec{F_E}\left(x,t\right)\right)\delta t \tag{13}$$

and (b) obtaining fluid-solid interaction force from the rate of momentum exchange, using intermediate velocity for fluid as:

$$\vec{F_H}\left(x,t\right) = \varphi\left(x,t\right)\rho\left(x,t\right)\frac{\left(\vec{u_p}\left(x,t\right) - \vec{u'}\left(x,t\right)\right)}{\delta t} \tag{14}$$

Here $\vec{u}_p(x,t)$ is the particle velocity. Now the velocity field of the whole domain is obtained as:

$$\vec{u}\left(x,t\right)=\vec{u'}\left(x,t\right)+\frac{\overrightarrow{F_H}\left(x,t\right)\delta t}{2\rho\left(x,t\right)} \tag{15}$$

SPM is used in TLBM in a similar manner as for LBM. Here a temperature field is defined for the whole computational domain as:

$$T\left(x,t\right)=\left(1-\varphi\left(x,t\right)\right)T_f\left(x,t\right)+\varphi\left(x,t\right)T_p\left(x,t\right) \tag{16}$$

Where, indices *f* and *p* show fluid and particle (solid) regions, respectively. Similar to SPM for the velocity field, an intermediate temperature field and the heat source/sink term is defined by

$$T'\left(x,t\right)=\sum_{i=0}^{8}g_i\left(x,t\right) \tag{17}$$

$$Q\left(x,t\right)=\varphi\left(x,t\right)\frac{\left(T_p\left(x,t\right)-T'\left(x,t\right)\right)}{\delta t} \tag{18}$$

Consequently, the corrected temperature field is given by

$$T\left(x,t\right)=\sum_{i=0}^{8}g_i\left(x,t\right)+\frac{1}{2}Q\left(x,t\right)\delta t \tag{19}$$

From the above equations, velocity and temperature distribution are obtained at any time step, starting from known initial values. However, an engineering parameter of interest is the rate of heat transfer which can be obtained if the Nusselt number is determined which is discussed in the next section.

2- 4- Averaged nusselt number

Nusselt number is defined based on convection heat transfer coefficient (h) , the thermal conductivity of the fluid (k) and a length scale which is selected as inner cylinder diameter as:

$$Nu=\frac{R_i h}{k} \tag{20}$$

With the above definition, Nusselt number is a local parameter as convection heat transfer coefficient depends on the specific location on the solid surface. Average Nusselt number ($\overline{Nu}$) over the surface Γ is defined as:

$$\overline{Nu}=-\frac{L\int\frac{\partial T}{\partial n}d\Gamma}{\left(T_h-T_c\right)\int d\Gamma} \tag{21}$$

2- 5- Natural convection simulation

In natural convection, fluid flow occurs due to the temperature gradient which, in turn, creates a density variation and consequently results in a buoyancy force to appear. Using Boussinesq approximation, this force, which is considered as an external force, $\vec{F}_E$ is written as:

$$\overrightarrow{F_E}\left(x,t\right)=\rho\left(x,t\right)\vec{g}\left(x,t\right)\beta\left(T\left(x,t\right)-T_{ref}\right) \tag{22}$$

where $\vec{g}$ is acceleration due to gravity, ρ is the density, T_{ref} is the reference temperature (cold wall or ambient temperature, usually set to 0 in the non-dimensional scale), T is the local temperature and β is the thermal expansion coefficient. It must be mentioned that the basis of Boussiness approximation is that there are flows in which the temperature varies little, and therefore the density varies little, yet in which the buoyancy drives the motion.

2- 6- Numerical algorithm

The solution procedure of SP-TLBM is performed as follows:

1. Compute the equilibrium distribution functions corresponding to the initial values using Eq. (2), and Eq. (7). Give the initial distribution functions as $f=feq$ and $g=g_{eq}$.
2. Compute the density field, velocity field and temperature field using Eq. (4), Eq. (13) and Eq. (17), respectively.
3. Compute the force term and heat source using Eq. (14) and Eq. (18).
4. Correct the velocity field using Eq. (15).
5. Correct the temperature field using Eq. (19).
6. Compute the discrete force and heat source terms using Eq. (3) and Eq. (8).
7. Compute the density and temperature distribution functions in the entire computational domain using Eq. (1) and Eq. (6) and return to step 2.

3- Results

The geometry considered in the present study is an annular region between the two cylinders. For the case of two concentric cylinders, this geometry is a standard one which has been studied by many authors. This section consists of a validation part, including computations for an annulus region between the two concentric cylinders followed by the results obtained for the case of eccentric cylinders.

Fig. 2 shows the flow geometry of a region between the two cylinders which are not concentric. Here two cylinders with radii of R_i and R_o are considered in which the inner cylinder has an eccentricity equal to *'E'*. The inner cylinder and outer cylinder surface temperature are kept at T_h and T_c respectively where $T_h=1$ and $T_c=0$. The range of Rayleigh number ($Ra=g\beta(T_h-T_c)L^3/\vartheta\alpha$), eccentricity ($e=E/(R_i-R_o)$) and radial ratio ($R_o/R_i$) are 10^3–10^5, $-0.75 \le e \le 0.75$, and $2 \le R_o/R_i \le 3.2$, respectively. The Prandtl number ($Pr=\vartheta/\alpha$) of the base fluid is kept constant at 0.716 corresponding to the air. In an annulus, the flow can be considered steady and laminar for Rayleigh numbers less than 10^6 [28]. The solution is converged when the maximum absolute error between the new and old values of the velocity field and the temperature field are less than 10^{-8}.

The computational grid is shown in Fig. 3, the schematic of the local computational grid is illustrated in Fig. 3, as well. As mentioned before the SPM defines a spatial indicator field which varies from 1 in the solid region to 0 in fluid region smoothly and this approach does not need to consider Lagrangian points on the solid boundary.

As a first simulation, annular region between the two

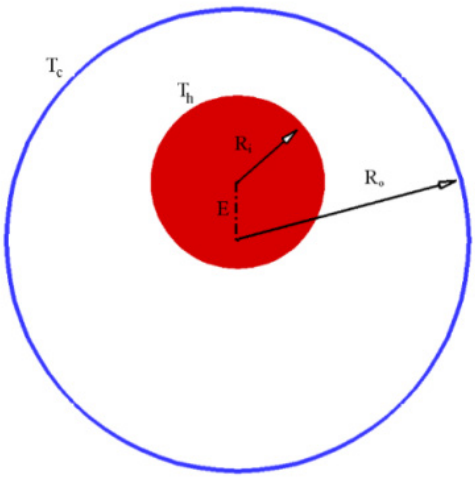

Fig. 2. The geometry of eccentric annulus

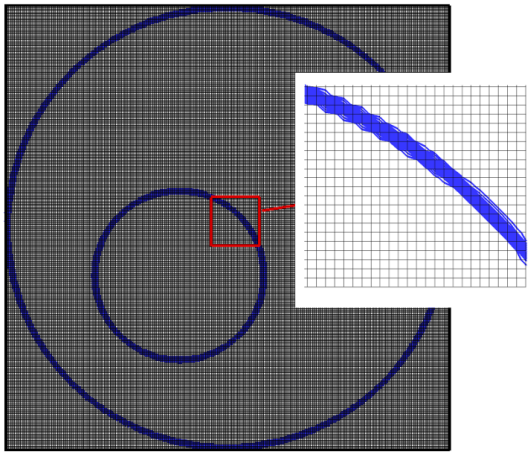

Fig. 3. Schematic of the local computational grid

concentric cylinders with R_o/R_i = 2.6 at Ra = 10^4 is studied to investigate the effect of the number of grid points on Nusselt number. For the grid independence, three different grids were used: 200×200, 300×300, and 400×400. The check of the grid independence based on the results of the mean Nusselt number Nu versus the Rayleigh number Ra for the three sizes of the grids is presented in Fig. 4. It is seen that there is no discrepancy between the results obtained from these three sizes of the grids; the solution being independent of the grids. Therefore, the grid size 300×300 is selected for the present computations.

To validate the present computational framework, the average Nusselt number is computed for the two concentric cylinders and compared with experimental and numerical results existing in the literature, cf. Table 1. Based on data presented in this table, a good correspondence is observed between present computations and those of Kuhen and Goldestien [2] and Shahraki [6]. Comparison of isotherms between the present study and experimental data obtained by Kuehn and Goldestin is presented in Fig. 5 for validation.

Fig. 6 shows a radial temperature distribution at four different angles for annulus regions of two concentric cylinders. Comparison with experimental data of Kuehn and Goldestin shows a good correspondence between present computational

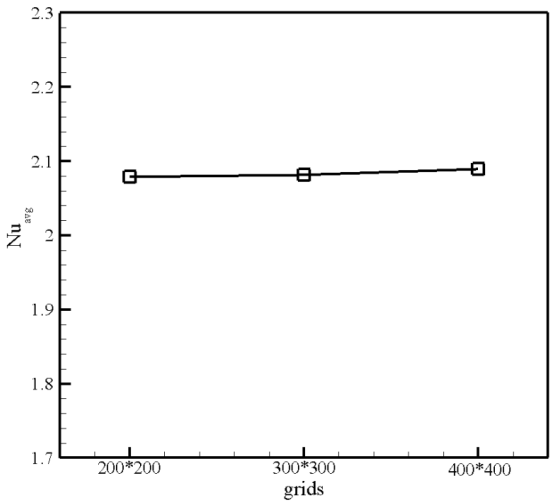

Fig. 4. Nu_{avg} for different grids (Pr=0.716 , ε=0, R_o/R_i =2.6, Ra=10^4)

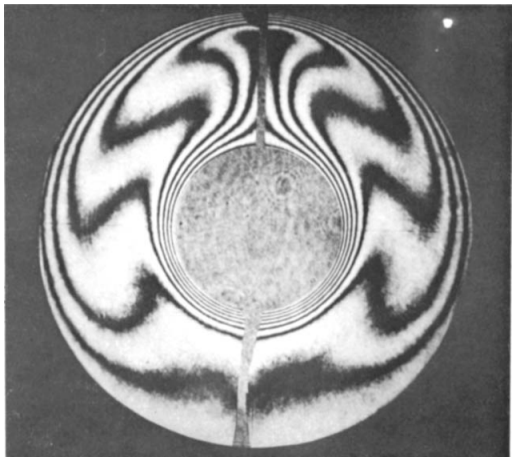

Kuehn and Goldstein (1976) , Experimental isotherms

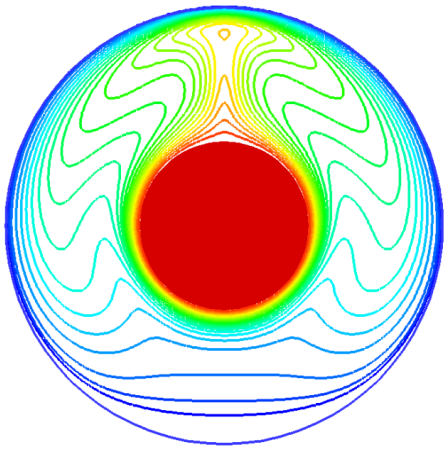

Present study , Numerical isotherms

Fig. 5. Comparison of isotherms between the present study and experimental data

results and experimental data. Please note that the angle θ is zero in a vertically upward direction and increases clockwise.

Table 1. Average Nusselt number for concentric cylinders (Pr=0.716 , R_o/R_i =2.6)

Rayleigh number	Present study	Experimental [K-G]	Numerical [Sh]
1.31×10^3	1.1881	1.14	1.1386
9.50×10^3	2.0537	2.01	1.9901
6.19×10^4	3.3056	3.32	3.3092
1.02×10^5	3.7285	3.66	3.6475

K-G: Kuehn and Goldestin (experimental data 1976), Sh: Shahraki (numerical results 2002)

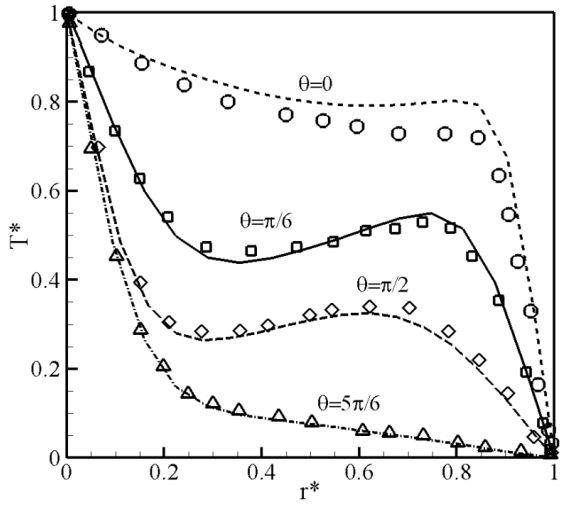

Fig. 6. Comparison of the temperature profiles at different angles (Pr=0.716, R_o/R_i =2.6 , Ra=5×10^4) Lines for the present study and symbols for experimental data

Table 2 shows the effect of various eccentricities on the average Nusselt number for Ra=10^5, radius ratio equal to 2.6 and Pr=0.716. It is observed that as eccentricity increases, the average Nusselt number decreases as a result of a reduction in convection portion in heat transfer against conduction. This behavior is not valid for e=0.8 due to the ascending of pure conduction effect in comparison with descending of natural convection influence. In other words, in this case, the plume region does not have enough space to grow, increase pure conduction, and overcome the effect of decreasing natural convection.

Table 2. Average Nusselt number for eccentric cylinders (Pr=0.716 , R_o/R_i =2.6 , Ra=10^5)

e	Present study	Experimental [K-G]
-0.8	4.1182	3.9504
-0.623	3.9011	3.7824
0	3.7096	3.6475
0.625	3.0665	3.1123
0.8	3.2141	3.2248

The influence of horizontal movement of the inner cylinder is presented in Figures 7 and 8. Figures 7 and 8 show the inner cylinder movement to the right and left, respectively. As shown, the behavior of streamlines and isotherms is thoroughly symmetrical regardless of the inner cylinder movement to the right or left direction. Therefore, the equal horizontal movement of the inner cylinder to the right and left direction does not influence the streamlines and isotherms patterns. However, for small horizontal eccentricities, two vortices can be identified on the two sides of the inner cylinder. As eccentricity increases, one of the vortices shrinks and the other expands. The vortices formation region represents the increase in convection portion versus conduction. Furthermore; by raising distance from the center, conduction quota against convection increases.

Figures 9 and 10 represent streamlines and isotherms for vertical displacement. As illustrated, streamlines and isotherms move toward the top of the inner cylinder to reach the outer cylinder. The fluid flow in the larger annulus space is faster. Consequently, convection is more dominant in this location. As the distance between inner and outer cylinder reduces, fluid velocity in this region declines. Therefore, vortices move slower in this zone and convection becomes less important than conduction. It can be shown that isotherms below the inner cylinder become horizontal. Instead, as eccentricity in downward direction (negative) increases, convection role in annulus space becomes evident. Moreover, high-temperature gradient is observed for all states.

Figures 11 and 12 represent streamlines and isotherms for diagonal inner cylinder motion. It can be concluded that they have the same behavior like the previous case (vertical displacement). The only difference is that the streamlines and isotherms are not symmetric.

The variation of average Nussselt number with eccentricity can be seen in Figure 13. For all cases, it can be observed that eccentricity variation affects average Nusselt number. There is a symmetrical behavior for horizontal movement. For eccentricity equal to -0.75, the highest Nusselt number is gained. This shows in this situation, convection is dominated in the larger part of the annulus. Also, for vertical and diagonal displacements, when the inner cylinder moves upward, the gap between the inner and the outer cylinders becomes narrow and as a result of this, convection becomes weak and Nusselt number decreases to a minimum. As can be seen from the figure, the inner cylinder position can affect the plume region and also the density of isotherms near the cylinders and as a result of it, the average Nussselt number varies for different positions. When the eccentricity gets a negative value, the space for growing the plume region increases and consequently the average Nussselt number is higher in this case.

The effect of the radial ratio (R_o/R_i) on the isotherms is illustrated in Figure 14 when Ra=10^4, e=-0.5 (vertical direction). It is observed that when the parameter R_o/R_i decreases the intensity of the temperature, variation near the cylinders increases and then enhances the thermal flux near the inner cylinder.

Figure 15 shows the average Nusselt number for different values of Radios ratio when Ra=10^4. As can be observed in Figure 15 for all of the radius ratios, the average Nusselt number is reduced by increasing eccentricity. This trend shows that the convection of the fluid inside the enclosure arises more easily in the case of negative eccentricities than when e is positive. It is in agreement with the results presented

e=-0.75

e=-0.5

e=-0.25

Streamline patterns Isotherm patterns

Fig. 7. Streamlines and Isotherms for horizontal eccentricity $Ra=10^4$, $Pr=0.71$ (negative ε)

in Figure 13, which confirm that the mean Nusselt number *Nu* for the case of negative eccentricities is greater than for the cases positive eccentricities. As can be seen from Figure 15, in the case of horizontal eccentricity, the variation of average Nusselt number is less sensitive to eccentricity when radius ratio is higher. The reason for this phenomenon is that for the lower radius ratio the region for natural convection is almost the same for all eccentricities.

e=0.25

e=0.5

e=0.75

Streamline patterns Isotherm patterns

Fig. 8. Streamlines and Isotherms for horizontal eccentricity $Ra=10^4$, $Pr=0.71$ (positive ε)

e=-0.75

e=-0.5

e=-0.25

Streamline patterns Isotherm patterns

Fig. 9. Streamlines and Isotherms for vertical eccentricity Ra=10⁴, Pr=0.71 (negative ε)

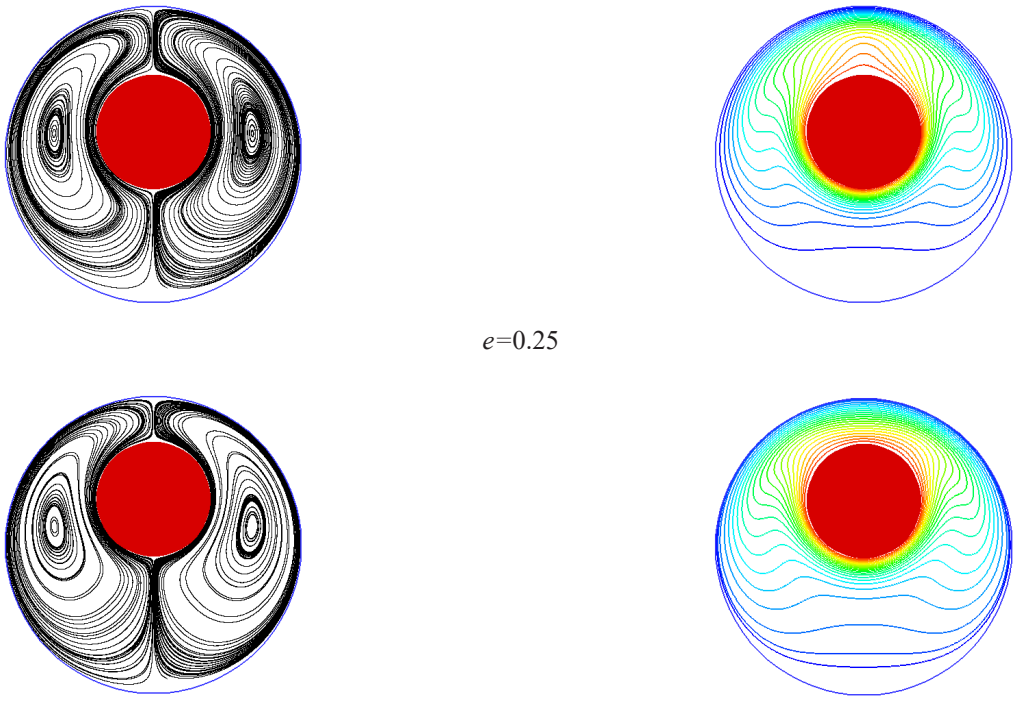

e=0.25

e=0.5

e=0.75

Streamline patterns Isotherm patterns

Fig. 10. Streamlines and Isotherms for vertical eccentricity Ra=10⁴, Pr=0.71 (positive ε)

e=-0.75

e=-0.5

e=-0.25

Streamline patterns Isotherm patterns

Fig. 11. Streamlines and Isotherms for diagonal eccentricity $Ra=10^4$, $Pr=0.71$ (negative ε)

e=0.25

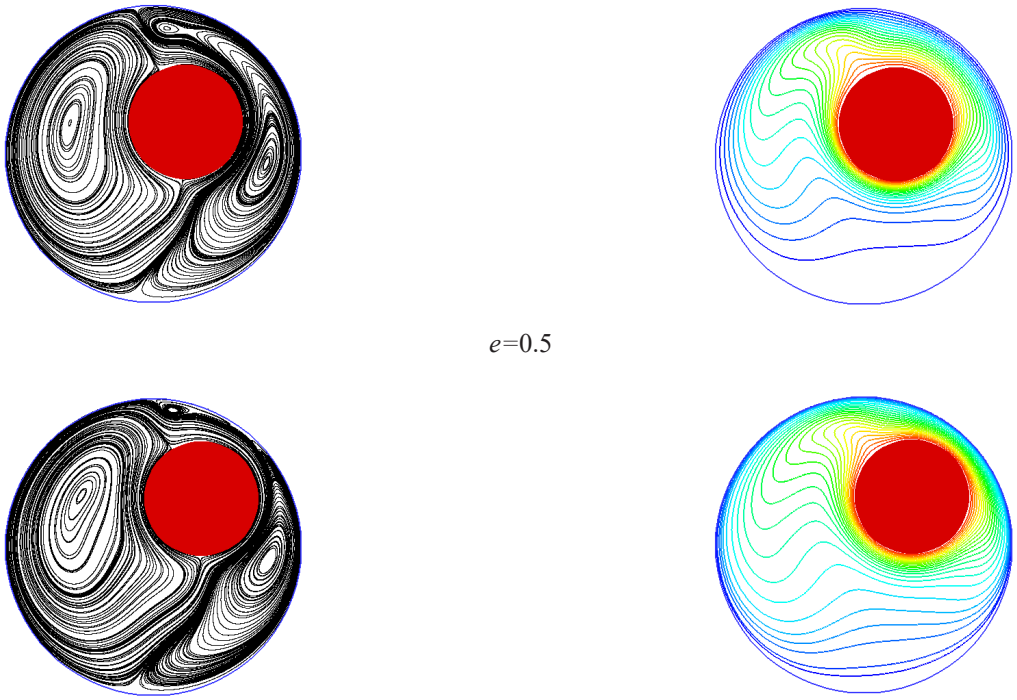

Fig. 10. Streamlines and Isotherms for diagonal eccentricity $Ra=10^4$, $Pr=0.71$ (positive ε)

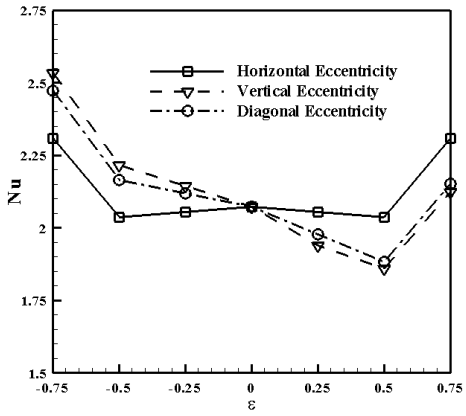

Fig. 13. Average Nusselt number versus eccentricity

Figure 16 presents the influence of Rayleigh number on isotherms when R_o/R_i=2.6, e=0.5 (in a diagonal direction). It can be observed when the Ra increases, the temperature gradients at the surfaces of the cylinders increase and as a consequence, the mean Nusselt number also increases. Also, it is observable that by increasing the Rayleigh number, the fluid movement occurs simply. Also when the Rayleigh number increases from 10^3 to 10^5, the larger plume appears on the inner cylinder. It is clear from Figure 17 that the average Nusselt number increases for higher Rayleigh numbers. It can be concluded that this phenomenon is independent of the direction of eccentricity. As the Rayleigh number increases, the main plumes of the isotherms ascends towards the outer cylinder, thermal boundary layer thickness decreases and it causes the Nusselt number to increase. As it is expected, there is a direct relation between *Nu* and *Ra*. As well as *Ra*

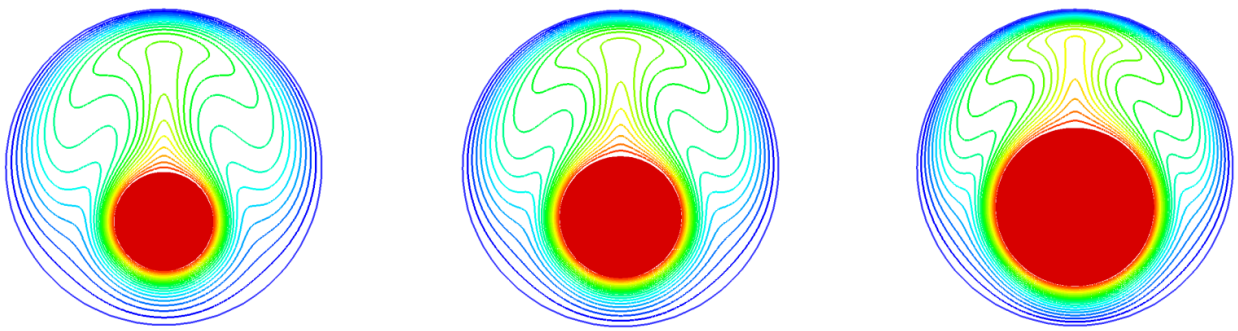

Fig. 14. Isotherms for different radial ratios ($Ra=10^4$, e=-0.5)

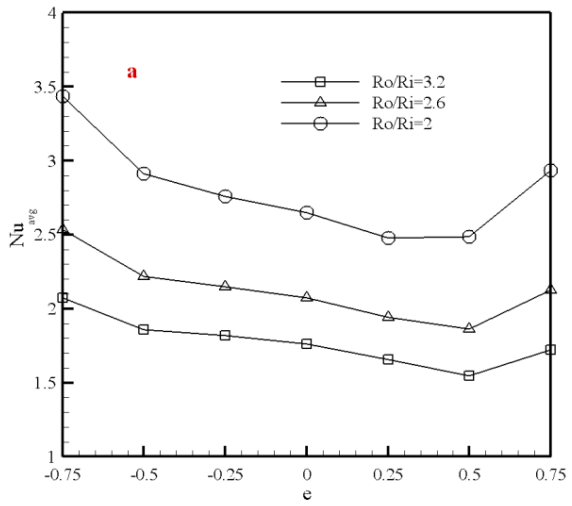

(a)

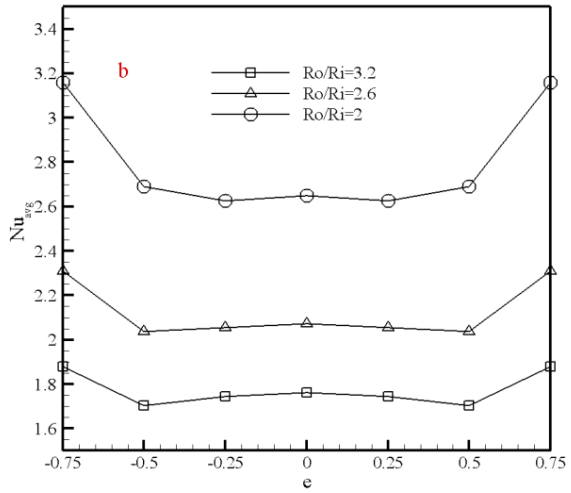

(b)

increases also *Nu* increases. This is due to the fact that an increase in *Ra* causes the increase in the buoyancy forces.

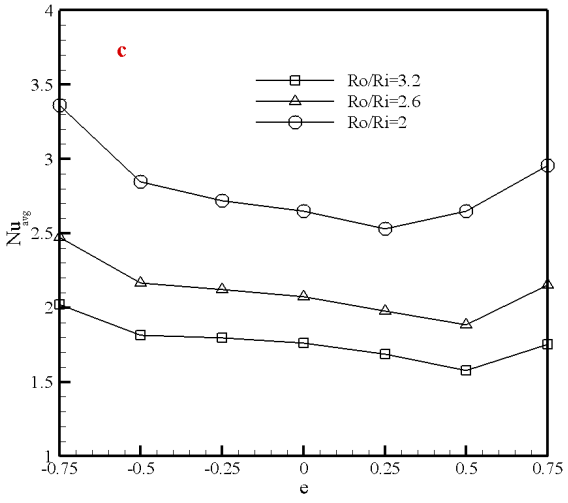

(c)

Fig. 15. The average Nusselt number for different values of Radios ratio when $Ra=10^4$. (a, b and c are corresponding to vertical, horizontal and diagonal eccentricities, respectively)

4- Conclusions

In the present study, SP-TLBM is employed as a forceful technique to simulate natural convection in an eccentric annulus. As all the calculations in SP-TLBM are conducted on Eulerian fluid nodes, this method is much simpler in contrast with the methods which use Lagrangian points on the surface of the curved boundary. The effects of Rayleigh number *Ra*, eccentricity e and radial ratio on streamlines, isotherms and Nusselt number are considered in this study. The inner cylinder position can change the structure of the flow and temperature fields. It is found that for equal absolute values of eccentricities in horizontal movement, the same behavior was observed for streamlines and isotherms in the annulus. The variation of Nusselt number versus eccentricity is almost identical for vertical and diagonal movement of the inner cylinder. In both cases, when the inner cylinder is located at the lowest level, the maximum Nusselt number is gained due to the existence of a powerful circulation in the annulus and the simplification of the fluid movement in space of the top of the inner cylinder. It is also found that eccentricity and radial ratio have a significant effect on the average Nusselt

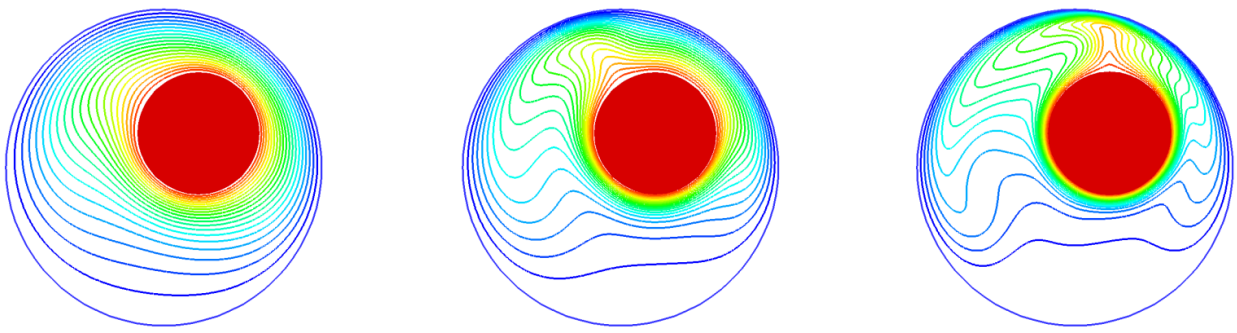

$Ra=10^3$ $Ra=10^4$ $Ra=10^5$

Fig. 16. Isotherms for different Rayleigh numbers (R_o/R_i=2.6 , e= 0.5)

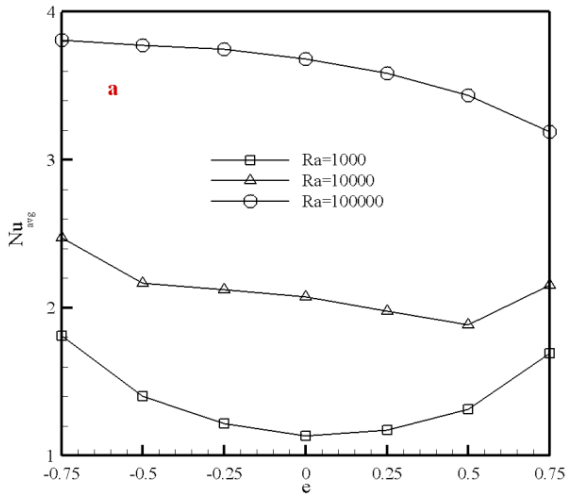

(a)

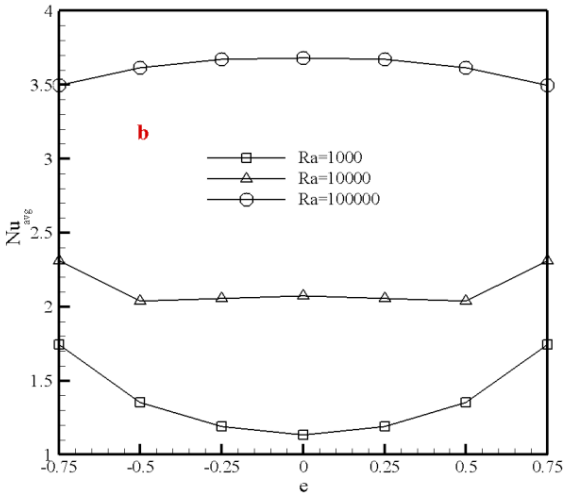

(b)

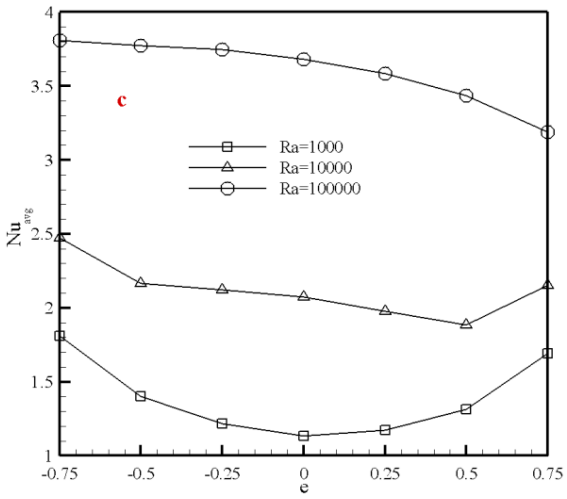

(c)

Fig. 17. The average Nusselt number for different Rayleigh numbers when R_o/R_i=2.6. (a, b and c are corresponding to vertical, horizontal and diagonal eccentricities, respectively)

number, especially for the higher *Ra* number. For the higher *Ra* numbers the buoyancy forces and the intensity of the plume increase and as a result of this, the Nusselt number also becomes higher.

References

[1] H. Dawood, H. Mohammed, N.A.C. Sidik, K. Munisamy, M. Wahid, Forced, natural and mixed-convection heat transfer and fluid flow in annulus: A review, *International Communications in Heat and Mass Transfer*, 62 (2015) 45-57.

[2] T. Kuehn, R. Goldstein, An experimental and theoretical study of natural convection in the annulus between horizontal concentric cylinders, *Journal of Fluid mechanics*, 74(4) (1976) 695-719.

[3] T.H. Kuehn, R. Goldstein, An experimental study of natural convection heat transfer in concentric and eccentric horizontal cylindrical annuli, *Journal of Heat Transfer*, 100(4) (1978) 635-640.

[4] T.H. Kuehn, R.J. Goldstein, A parametric study of Prandtl number and diameter ratio effects on natural convection heat transfer in horizontal cylindrical annuli, *Journal of Heat Transfer*, 102(4) (1980) 768-770.

[5] G. Guj, F. Stella, Natural convection in horizontal eccentric annuli: numerical study, *Numerical Heat Transfer, Part A: Applications*, 27(1) (1995) 89-105.

[6] F. Shahraki, Modeling of buoyancy-driven flow and heat transfer for air in a horizontal annulus: effects of vertical eccentricity and temperature-dependent properties, *Numerical Heat Transfer: Part A: Applications*, 42(6) (2002) 603-621.

[7] S. Succi, S. Succi, *The lattice Boltzmann equation: for fluid dynamics and beyond*, Oxford university press, 2001.

[8] Z. Guo, C. Shu, *Lattice Boltzmann method and its applications in engineering*, World Scientific, 2013.

[9] C.K. Aidun, J.R. Clausen, Lattice-Boltzmann method for complex flows, *Annual review of fluid mechanics*, 42 (2010) 439-472.

[10] X. He, S. Chen, G.D. Doolen, A novel thermal model for the lattice Boltzmann method in incompressible limit, *Journal of Computational Physics*, 146(1) (1998) 282-300.

[11] X. Shan, Simulation of Rayleigh-Bénard convection using a lattice Boltzmann method, *Physical Review E*, 55(3) (1997) 2780.

[12] Y. Wei, H.-S. Dou, Z. Wang, Y. Qian, W. Yan, Simulations of natural convection heat transfer in an enclosure at different Rayleigh number using lattice Boltzmann method, *Computers & Fluids*, 124 (2016) 30-38.

[13] Y. Peng, Y. Chew, C. Shu, Numerical simulation of natural convection in a concentric annulus between a square outer cylinder and a circular inner cylinder using the Taylor-series-expansion and least-squares-based lattice Boltzmann method, *Physical Review E*, 67(2) (2003) 026701.

[14] S. Dash, T. Lee, H. Huang, Natural convection from an eccentric square cylinder using a novel flexible forcing IB-LBM method, *Numerical Heat Transfer, Part A: Applications*, 65(6) (2014) 531-555.

[15] T. Seta, Implicit temperature-correction-based immersed-boundary thermal lattice Boltzmann method for the simulation of natural convection, *Physical Review E*, 87(6) (2013) 063304.

[16] Y. Shi, T. Zhao, Z. Guo, Finite difference-based lattice Boltzmann simulation of natural convection heat transfer in a horizontal concentric annulus, *Computers & Fluids*, 35(1) (2006) 1-15.

[17] E. Sourtiji, D. Ganji, S. Seyyedi, Free convection heat transfer and fluid flow of Cu–water nanofluids inside a triangular–cylindrical annulus, *Powder Technology*, 277 (2015) 1-10.

[18] M. Afrand, Using a magnetic field to reduce natural convection in a vertical cylindrical annulus, *International Journal of Thermal Sciences*, 118 (2017) 12-23.

[19] Z. Guo, C. Zheng, B. Shi, An extrapolation method for boundary conditions in lattice Boltzmann method, *Physics of Fluids*, 14(6) (2002) 2007-2010.

[20] E. Fattahi, M. Farhadi, K. Sedighi, Lattice Boltzmann simulation of natural convection heat transfer in eccentric annulus, *International journal of thermal sciences*, 49(12) (2010) 2353-2362.

[21] C.S. Peskin, Flow patterns around heart valves: a numerical method, *Journal of computational physics*, 10(2) (1972) 252-271.

[22] X. Niu, C. Shu, Y. Chew, Y. Peng, A momentum exchange-based immersed boundary-lattice Boltzmann method for simulating incompressible viscous flows, *Physics Letters A*, 354(3) (2006) 173-182.

[23] Z.-G. Feng, E.E. Michaelides, Proteus: a direct forcing method in the simulations of particulate flows, *Journal of Computational Physics*, 202(1) (2005) 20-51.

[24] H. Jeong, H. Yoon, M. Ha, M. Tsutahara, An immersed boundary-thermal lattice Boltzmann method using an equilibrium internal energy density approach for the simulation of flows with heat transfer, *Journal of Computational Physics*, 229(7) (2010) 2526-2543.

[25] S. Jafari, R. Yamamoto, M. Rahnama, Lattice-Boltzmann method combined with smoothed-profile method for particulate suspensions, *Physical Review E*, 83(2) (2011) 026702.

[26] Y. Nakayama, R. Yamamoto, Simulation method to resolve hydrodynamic interactions in colloidal dispersions, *Physical Review E*, 71(3) (2005) 036707.

[27] Y. Hu, D. Li, S. Shu, X. Niu, An efficient smoothed profile-lattice Boltzmann method for the simulation of forced and natural convection flows in complex geometries, *International Communications in Heat and Mass Transfer*, 68 (2015) 188-199.

[28] M.-I. Char, Y.-H. Hsu, Comparative analysis of linear and nonlinear low-Reynolds-number eddy viscosity models to turbulent natural convection in horizontal cylindrical annuli, *Numerical Heat Transfer, Part A Applications*, 33(2) (1998) 191-206.

Please cite this article using:

S. Jafari, S. Jafari, M. Rahnama, Simulation of Natural Convection in Eccentric Annulus: A Combined Lattice Boltzmann and Smoothed Profile Approach, *AUT J. Mech. Eng.*, 2(1) (2018) 13-26.

DOI: 10.22060/mej.2017.13013.5500